Geomechanics and Engineering, *Vol. 27, No. 3 (2021) 239-251*
https://doi.org/10.12989/gae.2021.27.3.239

Study on mechanical properties and damage features of Rock-Coal-Rock combination models with defects and fillings

Han D. Liu[1a], Shuai Liu[*1,2], Zhi G. Xia[**3], Jing J. Liu[2b], Hao Guo[4] and Yong T. Yuan[5]

[1]*Henan Key Laboratory of Geomechanics and Structural Engineering, North China University of Water Resourcesand Electric Power, Zhengzhou, 450045, China*
[2]*College of Geosciences and Engineering, North China University of Water Resources and Electric Power, Zhengzhou, 450045, China*
[3]*School of Mining Engineering, University of Science and Technology Liaoning, Anshan, 114051, China*
[4]*Liaoning Metallurgical Geological Exploration Team 405 Co., Ltd, Liaoyang, 111000, China*
[5]*Hami energy security monitoring center of Xinjiang Uygur Autonomous Region, Hami, 839000, China*

(Received April 15, 2021, Revised October 2, 2021, Accepted October 22, 2021)

Abstract. In order to study the damage features and mechanical properties of rock-coal-rock combination (RCR) models with defects and filling material, the 2-Dimensional Particle Flow Code (PFC2D) is used for the numerical simulation models. The variations of stress-strain, caused by uniaxial compression, are investigated. The distribution of the stress and displacement fields in horizontal and vertical directions of the models after failure is analyzed. The damage characteristics are discussed from the microscopic aspects of crack development, acoustic emission and contact force distribution. The results show the following: (1) The defects significantly affect the mechanical properties, the propagation of internal cracks, the evolution of displacement and stress and the distribution of stress concentration area. The peak stress-strain and elastic modulus of RCR models with defects decrease as the number of square holes increases. The more defects, the earlier new cracks appear in the coal body and the easier the defective models fail. (2) After filling the holes of the defective models, the number of cracks, crack initiation stress, elastic modulus and peak stress-strain are significantly larger than those of the corresponding model with holes, meaning that they can sustain larger load. The displacement and stress fields of the filled models are similar to the ones of the complete combination model. Hence, the filling material can enhance the mechanical properties of the defective RCR combination models.

Keywords: damage; flaw filling; mechanical properties; PFC2D simulation; Rock-Coal-Rock combination; weak interlayer

1. Introduction

There are some macro defects in the natural rock mass, such as weak interlayers and joints, as well as some micro defects, such as holes and micro-cracks (Helgeson and Aydin 1991, Tropeano *et al.* 2004), as shown in Fig.1. The existence of these defects directly affects the strength and mechanical properties of the rock, resulting in great dispersion and uncertainty in both meso-fracture mechanism and macro mechanical properties (Klein and Reuschle 2004, Nick *et al.* 2011, Tian *et al.* 2017, Liu *et al.* 2019a, Sharafisafa *et al.* 2020). The phenomenon of coal-rock interbedding is often encountered in the excavation of underground engineering projects, such as tunnels, mining and water conservancy projects. Some thin coal seams exist in hard rock layers, which are regarded as weak interlayers. The numerous defects, such as cracks and holes, are distributed inside the coal-rock mass, rendering its physical and mechanical behavior extremely complicated (Martin *et al.* 2003, Lollino *et al.* 2015, Marinelli and Buscarnera 2019). It is valuable to research the mechanical properties and damage features of coal-rock combinations in order to proceed to appropriate strengthening measures for the defective rock masses.

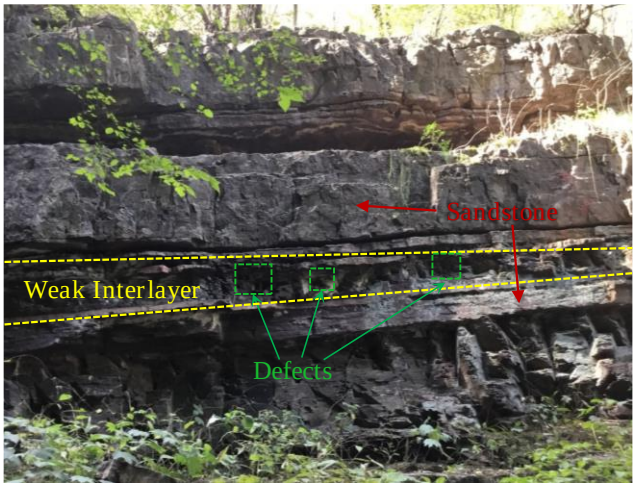

Fig. 1 Defective rock combination mass. The strata are the upper Permian, and the weak interlayer is carbonaceous mudstone. It is located in Pingdingshan City, Henan Province, China

∗Co-Corresponding author, Ph.D.
E-mail: austin-shuai-liu@qq.com
∗∗Co-Corresponding author, Ph.D.
E-mail: 514579197@qq.com
[a] Ph.D., Professor
[b] Ph.D.

ISSN: 2005-307X (Print), 2092-6219 (Online)

In recent years, scientists have performed many researches on the mechanical and damage characteristics of the coal-rock combinations either as defective rock mass or with filling material. The methods of numerical simulation and laboratory test are mainly used to study the rock-coal combination (Hawkes and Mellor 1970, Holt *et al.* 2005, Mondal *et al.* 2019). Liu *et al.* (2018) established different coal-rock combination models to study their mechanical properties and damage constitutive laws using compression experiments and damage mechanics theory; Yin *et al.* (2018) investigated combination models with given joint dip angles and different coal-rock height ratios, in order to determine their mechanical characteristics under different height ratios; Zuo *et al.* (2011) found that coal-rock combination is mainly damaged inside the coal sample due to compression. Many other researchers (Guo *et al.* 2018, Liu *et al.* 2019b, Lisjak *et al.* 2014) discussed the mechanical properties of such combination masses taking into account different coal sample heights and dip angles of structural planes. They used numerical analyses and provided many in-depth studies on their failure mechanism. Hazzard, Wu *et al.* (Hazzard and Young 2000, Hadjigeorgiou *et al.* 2009, Potyondy 2015, Wu *et al.* 2020, Wu *et al.* 2021) have also made some progress in reasonable modeling and parameter determination of particle flow numerical simulation code, which has strengthened the application of numerical simulation in rock mechanics. In terms of defective rock masses, the research mainly focuses on hard rock, with damage mechanics and theoretical mechanics as the theoretical support (Lajtai 1974, Cauvin and Testa 1999, Mikl-Resch *et al.* 2015). Defect types are mainly cracks of different scales, regular-shaped holes or a combination of holes and cracks (Kranz 1979, Klein *et al.* 2004, Park and Bobet 2009, Komijani *et al.* 2019). The research on the development of internal cracks in rock mass is often focused on the defect types dominated by cracks, and the fracture analysis method has also made great progress (Kim *et al.* 2015, Brandtner-Hafner 2021). Hillerborg (1976, 1985) conducted an in-depth study on the formation and propagation of cracks in concrete and determined the fracture energy GF; Ayatollahi and Akbardoost (2014) analyzed the effect of size and geometry on fracture toughness in mode I fracture. Vasarhelyi et al. (Vasarhelyi *et al.* 2000, Bahaaddini *et al.* 2013, Bahrani *et al.* 2016) also conducted numerical simulations on the crack development and mechanical properties of defective rock masses under compression. A lot of achievements have been made in the research on rock defects with regular holes (circular, triangular, oval, etc.) or combined with fractures (Wong *et al.* 2006, Jespersen *et al.* 2010, Zhou *et al.* 2017). For example, a systematic study on the crack evolution, deformation ruler and strength characteristics of rock with voids and fractures can be found in (Yang *et al.* 2017, Chen *et al.* 2020), revealing the dynamics and failure mechanisms of the rock containing void defects. Gui *et al.* (2017) analyzed the influence of triangular, rectangular andcircular holes on the mechanical behavior of rock samples; Fakhimi *et al.* (2002) used PFC2D simulation to reproduce the damage zone of the circular hole rock in the laboratory test. In the study of filling rock mass, through laboratory tests and CT scanning, Janeiro *et al.* (2010) conducted uniaxial compression tests on gypsum samples with different numbers, strengths, and shapes of inclusions to compare the shear crack growth degree with different numbers of inclusions; Xia *et al.* (2020) used PFC2D to study the stress-strain relation and the damage evolution of rocks with cavities of various shapes, subjected to uniaxial compression, obtaining the stress concentration range and failure modes of both defective and filled models; Komurlu *et al.* (2016) based on the concept of crack initiation and fracture toughness under different loading conditions, and determined the best indirect tensile strength of cement paste filling materials; Strmsvik *et al.* (2020), Moradi *et al.* (2021) used grouting technology to fill the voids of tunnel surrounding rock with cement mortar and other materials to strengthen the rock mass, so as to improve the stability of the tunnel.

The above researches mainly focus on the mechanical characteristics and damage mechanisms of the combination with different coal thicknesses, dip angles and combination modes. Furthermore, defective and filled models of rock mass are often studied, while similar models of coal-rock combination are not yet sufficiently investigated, and its damage characteristics need further study. In fact, holes and other defects may have a more serious impact on coal or other weak interlayers than on rock (Haimson and Kovacich 2003, Esterhuizen *et al.* 2011). This paper utilizes the particle flow code to establish the numerical models of rock-coal-rock combinations with square cavity defect and filling in coal interlayer, and study their mechanical and failure characteristics.

2. Numerical parameters and model establishment

2.1 The particle flow code and parameter determination

PFC2D (2-Dimensional Particle Flow Code) is an effective scientific method, suitable to analyze the meso characteristics of the failure process of the rock, such as the number of cracks and the crack propagation. It is a common tool for macro-meso-research of rock mechanics (Potyondy and Cundall 2004, Yang *et al.* 2006). It is used to simulate the connection between rock particles, which is usually represented by parallel contact bonds (Cundall and Strack 1979). In this study, the parallel bond model is adopted to establish the rock-coal-rock combination with different defects and filling material, which assumes a contact force between the particles of the mass that enables the transferring of forces, moments and displacements. When the maximum tensile and shear stresses of the parallel bonds between rock particles reach the corresponding strengths of the bond, the particle bonding fails. This method can determine the micro parameters of particles, which cannot be accurately obtained from laboratory tests. In order to have reliable and reasonable numerical results, the basic mechanical parameters, such as elastic modulus of rock and coal masses, are derived from a series of laboratory tests. The laboratory tests use The Shimadzu AG-

Table 1 Microscopic parameters of Rock, Coal and Filling material

Parameters	Rock	Coal	Filling material
Minimum particle diameter (mm)	0.3	0.3	0.3
Particle diameter ratio	1.5	1.5	1.6
Density (kg/m^3)	2650	1300	1470
Contact modulus of the particle (GPa)	9.3	1.62	1.32
Contact bond gap (mm)	0.05	0.05	0.05
Porosity	0.1	0.1	0.1
Parallel bond friction angle (°)	37	29	35
Parallel bond tensile strength (MPa)	23.3	2.27	3.5
Normal critical damping ratio	0.5	0.5	0.5
Parallel bond cohesive force (MPa)	31.5	4.92	6.3

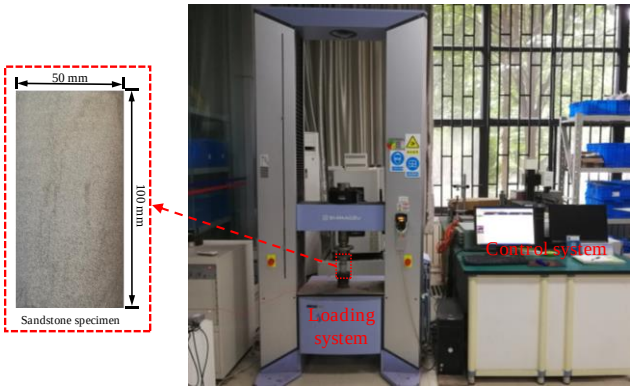

Fig. 2 The test machine and size diagram of standard cylindrical rock specimen

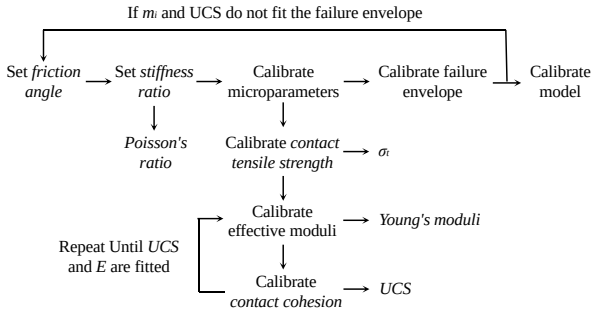

Fig. 3 Uniaxial compression calibration procedure

X250 precision universal test machine, which can perform uniaxial compression and shear tests of rock. The test results are reliable and accurate. The uniaxial compression test is carried out using the displacement loading control method until the rock sample is broken, and the loading rate is set at 0.01mm/s. The samples are standard cylindrical sample (φ50mm×100mm), and all tests are carried out in accordance with ISRM standards (Brown 1981, Fairhurst *et al.* 1999). The laboratory tests equipment and rock sample specifications are shown in Fig.2. On the basis of laboratory tests, a series of numerical simulation tests similar to laboratory test conditions were carried out. The numerical and experimental results are compared and adjusted if necessary until the micro parameters meet the requirements (Castro-Filgueira *et al.* 2017, Wang *et al.* 2020). Fig.3 illustrates the process of parameter checking in PFC method.

Based on a large amount of laboratory tests, the micro parameters are checked and the results are shown in Fig.4. It can be noted that there are some small errors in the maximum strain of the experimental sample and the corresponding numerical one, but the elastic modulus and strength are basically equal. The microscopic parameters of the PFC models meet the test requirements. Table 1 shows the micromechanical parameters of rock and coal samples and filling material based on PFC analysis.

2.2 Establishing the numerical models

A 2D Rock-Coal-Rock (RCR) model is established to study the damage features and mechanical properties of the combination containing defects and filling material. The complete combination model has height and width of 100 mm. The coal sample is located in the middle of the rock mass, with height 20 mm and width 100 mm. The square hole-defect, with dimensions 20 mm×20 mm, is assumed to be located inside the coal body. Three cases are considered with one, two or three square holes or filling material, evenly distributed in the width of coal body, as shown in Fig.5. For the simulation of the hole-defects, the particles of the corresponding size are deleted from the model, while for the filled sample these holes are replenished with the appropriate material. Seven numerical models are created, including the complete model A without holes, the defective model B-1 with one hole and the corresponding filled one B-2, the defective model C-1 with two holes and the corresponding filled one C-2 and finally the defective model D-1 with three holes and the corresponding filled one D-2. Fig.5(a) illustrates the complete model showing also the loading scheme of uniaxial compression. The models B, C and D are shown in Figs.5 (b) to (d), respectively.

3. Numerical analyses

3.1 Numerical simulation procedure

The stress-strain curves for each model are shown in

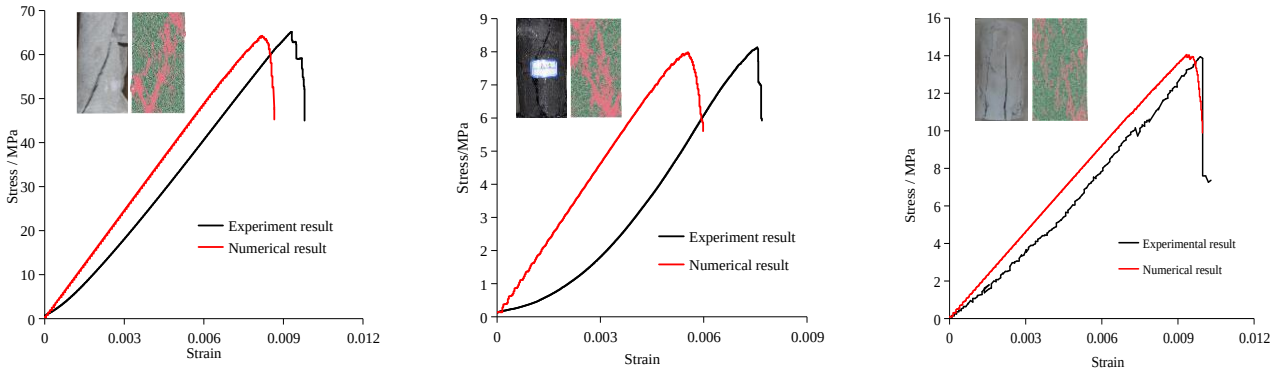

(a) Rock specimen (b) Coal specimen (c) Filling material

Fig. 4 Comparison of stress-strain curves between experimental specimens and numerical models under uniaxial compression

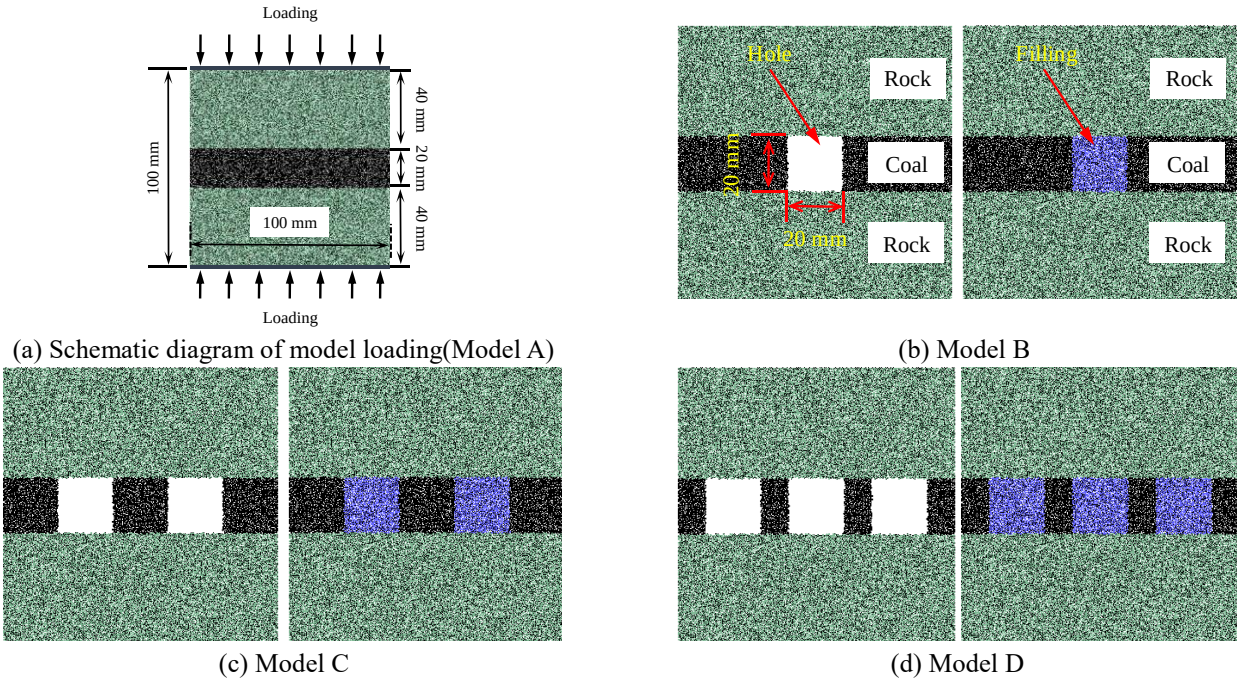

(a) Schematic diagram of model loading(Model A) (b) Model B

(c) Model C (d) Model D

Fig. 5 Numerical models and schematic diagram of model loading

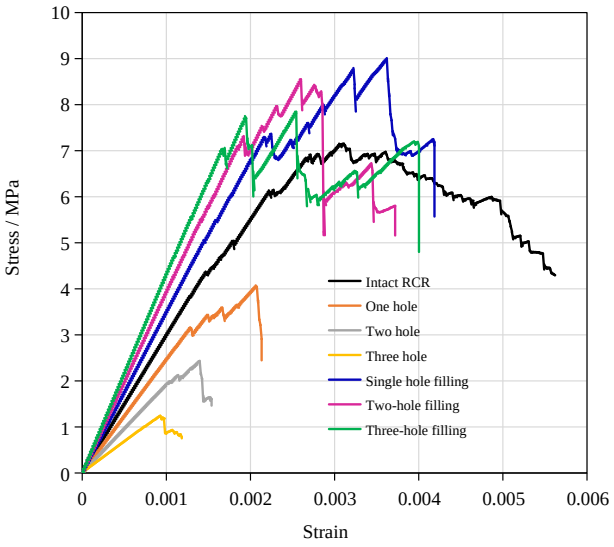

Fig. 6 Stress-strain curve of each model

Fig.6, while the peak value curves are plotted in Fig.7. As shown in these Figures, the peak stress, peak strain and modulus of elasticity for model A are 7.11 MPa, 3.05e-3 and 2.33 GPa, respectively. The stress-strain curve evolves linearly for small strains and it becomes corrugated after reaching the yield stress, mainly because the coal body is much weaker than the rock mass. As noted in Fig. 7, compared with model A, the stress and strain peak values as well as the modulus of elasticity for the defective models are significantly reduced. For instance, the reduction for model D-1 arises at 83.4%, 69.0% and 45.9%, respectively. The number of holes affects the mechanical properties of the RCR combination, as the increase of their numbers leads to the reduction of the samples' strength.

Compared with model A, the stress-strain curves of the filled models fluctuate before and after the peak value, as shown in Fig.6. It starts almost linear, but as the strain increases it becomes irregular and sawtooth, because the three materials have different mechanical properties and

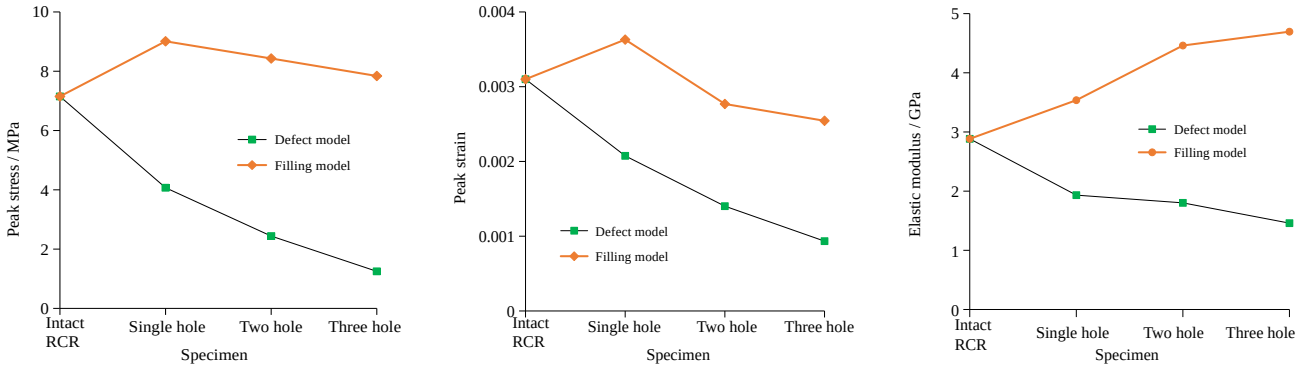

(a) Peak stress (b) Peak strain (c) Elastic modulus

Fig. 7 Peak value curves of defective and filled models

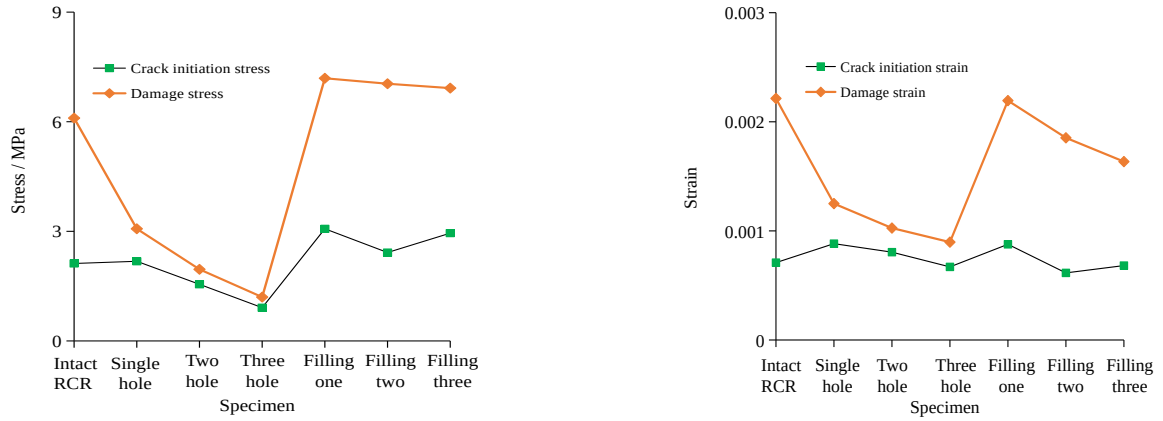

(a) Crack initiation and damage stresses (b) Crack initiation and damage strains

Fig. 8 The line chart of crack initiation and damage stresses and strains

their stress-strain states are inconsistent. The peak values and elastic modulus of the filled samples are larger than the ones of model A, as the mechanical properties of the filling material are better than those of the coal sample. The peak stress and strain as well as the modulus of elasticity for model B-2 increase by 123.4%, 77.5% and 25.9%, respectively, compared with model B-1. Comparing model C-2 with model C-1, an increase of 269.2%, 96.2% and 73.7% is noted for peak stress, peak strain and modulus of elasticity, respectively. Similarly, the increase between models D-2 and D-1 reach 557.6%, 165.9% and 145.2%, respectively.

The above analysis shows that the existence of defects has an important impact on the mechanical properties of the RCR combination, reducing the values of the peak stress and strain as well as the elastic modulus. With the increase of holes' number, the values of the peak stress-strain for the RCR combination model gradually decreases, as the sample becomes weaker. However, the filling material added in the holes improves the mechanical properties of the RCR combination samples.

3.2 Analysis of crack initiation stress and damage stress

Crack initiation and damage stresses are important values that determine the rock's strength and define thresholds of different stages of crack propagation. The crack initiation stress represents the stage when new cracks appear and expand. At this time, the cracks are still at a stable state. The damage stress indicates that the micro-cracks expanded in the previous stage rapidly converge and interconnect, causing an unstable propagation until the peak stress of the rock is reached (Molladavoodi *et al.* 2011, Pepe *et al.* 2017). This work utilizes the method of monitoring micro-cracks to determine the crack initiation and damage stresses, which, according to scientific studies (Eberhardt *et al.* 1998, Pelli *et al.* 1991), gives results almost equal to the experimental ones. Fig.8 and Table 2 provide the crack initiation and damage stress and strain values for each model for the RCR combination.

In Fig. 8(a) it is shown that the crack initiation stresses decrease gradually as the number of square holes increases in the defective models, meaning that the more defects are detected, the earlier the cracks begin. After the defective models are filled, the crack initiation stresses increase with values larger than the ones of model A, indicating that the filling material can inhibit the occurrence and development of new cracks. The damage stresses of all defective models is smaller than the ones of model A, resulting in smaller values as the number of square holes increases. The damage stresses of the filled model are larger than those of model A,

Table 2 Specific values of crack initiation and damage stresses and strains of specimens

Category	Crack initiation stress (MPa)	Damage stress (MPa)	Crack initiation strain (10^{-3})	Damage strain (10^{-3})
Model A	2.12	6.1	0.709	2.214
Model B-1	2.18	3.07	0.883	1.250
Model C-1	1.55	1.96	0.805	1.026
Model D-1	0.911	1.20	0.670	0.897
Model B-2	3.07	7.19	0.877	2.194
Model C-2	2.42	7.04	0.615	1.853
Model D-2	2.95	6.92	0.682	1.635

showing an increase of 4.12 MPa, 5.08 MPa and 5.75 MPa, respectively, compared with the corresponding defective models. This indicates that the filling material added in the holes can increase the stability of the combination mass with defects. In Fig.8 it is noted that the change trend of the stresses is consistent with the one of the strains, for both crack initiation and damage curves, being also consistent with the change trends of the peak stress and strain curves of Fig. 7.

3.3 Characteristics of the model failure and contact force distribution

As the load increases, cracks gradually appear and grow slowly, but after the peak strength is reached the number of cracks increases suddenly and finally the specimen fails. In order to study the crack propagation in the specimens, the number of the cracks is measured as the load increases. The results are presented in Fig.9, by means of crack number-strain curve and total number of cracks after failure. Fig.9 (b) shows the number of cracks when the model strength is half of the peak strength. The curve in Fig.9(a) shows that the crack development of both defective and filled models goes from the stage of crack free to initial crack appearance with slow growth and finally to rapid growth due to failure. In the original loading stage, the cracks do not open because of the small stress. As the load increases, cracks appear gradually and grow slowly. After the peak strength is reached the crack propagation becomes faster. In Fig.9 it is noted that the stresses, strains and the number of cracks at the final stage, when the models fail, are smaller for all defective and filled models than the ones for model A. Moreover, they are smaller for the defective models than for the filled ones. The overall shape of the crack number curves for the filled models is similar to the one of model A, but the fluctuation is large. The main reason is that the growth order of the cracks is not consistent in both coal and filling materials, as first, they appear in the coal body and then in the filling material.

As the load increases, cracks gradually appear and grow slowly, but after the peak strength is reached the number of cracks increases suddenly and finally the specimen fails. In order to study the crack propagation in the specimens, the number of the cracks is measured as the load increases. The results are presented in Fig.9, by means of crack number-strain curve and total number of cracks after failure. The curve in Fig.9(a) shows that the crack development of both defective and filled models goes from the stage of crack free to initial crack appearance with slow growth and finally to rapid growth due to failure. At the first steps of the loading process, the cracks do not open because of the small stress. As the load increases, cracks appear gradually and grow slowly. After the peak strength is reached the crack propagation becomes faster. In Fig.9 it is noted that the stresses, strains and the number of cracks at the final stage, when the models fail, are smaller for all defective and filled models than the ones for model A. Moreover, they are smaller for the defective models than for the filled ones. The overall shape of the crack number curves for the filled models is similar to the one of model A, but the fluctuation is large. The main reason is that the growth order of the cracks is not consistent in both coal and filling materials, as first, they appear in the coal body and then in the filling material.

Fig.10 shows the distribution of failure and contact force for each model, in which the red force chains represent pulling stresses and the blue ones compression stresses. As the stress concentration increases, the force chain in the parallel contact force distribution diagram becomes denser and the color deeper. In Fig.10(a) it is noted that the stress concentration under uniaxial compression is mainly distributed in the coal layer and the stress during damage is concentrated at the center of the whole sample in the form of two ends in a divergent “fascicular” shape. The coal sample center is the compression stress concentration area and its two ends constitute the tensile stress concentration areas. Compared with model A, the tensile stresses in the defective models are also concentrated in the coal body, occupying a smaller area as the number of square holes increases. As the load increases, the compression stress gradually moves outward. The medium pressure stress of defective models B and C is concentrated on both sides of the holes and the bundles of force chains are formed around the coal body at both ends. The pressure stress of the defective model D mainly exists in the “coal pillars”, formed around the three holes and the surrounding rock mass. From the above analysis, it can be concluded that the existence of defects changes the distribution of contact force, resulting in a change of the location and the size of compression and pulling stress concentration areas in the models. When the models fail, the stress concentration degree gradually decreases as the number of the holes increases. As the contact force distribution becomes more dispersed, the load-bearing capacity of the models gradually

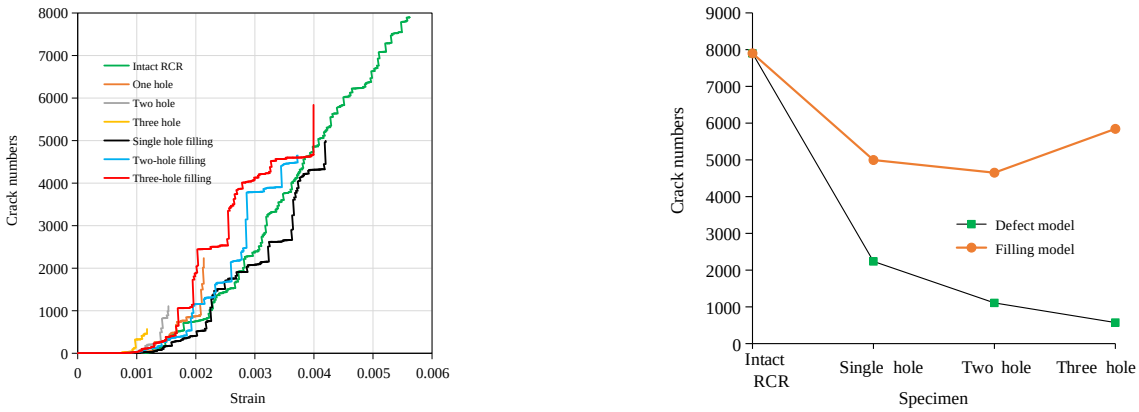

(a) Crack number-strain curve (b) The model failure crack number

Fig. 9 Crack number strain curve of each model and crack number of failure model

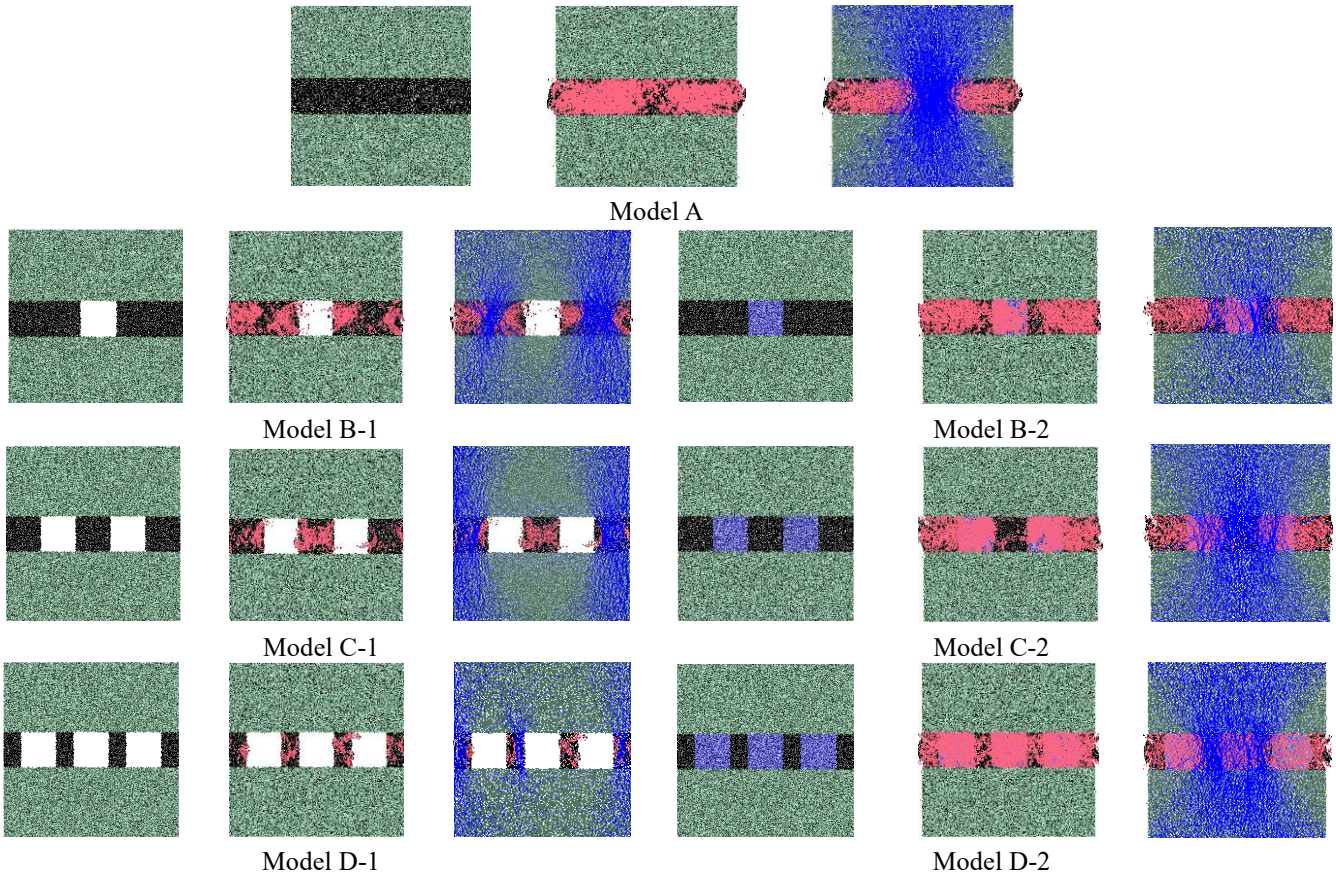

Fig. 10 Failure model and contact force distribution

decreases. Compared with the defective models,the stress chains of the filled models are denser, the tensile stresses are evenly distributed in the coal sample and the compression stresses are concentrated at the center of the models. The compression stress distribution of the filled model C and D are similar to, but slightly sparser than the one of the model A. This indicates that the load-bearing capacity of the filled models is greatly improved with respect to the one of the defective models.

3.4 Acoustic emission (AE) characteristics of models

Based on the occurrence of cracks in PFC, the acoustic emission (AE) of the specimen is defined. The number of AE shots is derived from the breakage of bonds (Komijani *et al.* 2020, Wang *et al.* 2021). Fig.11 shows the stress-strain curves along with the AE event counts for the models with defects and filling material. The variations of AE shots of the defective models B, C and D are similar under uniaxial compression. During the initial loading stage, when the stress and strain are small, no AE events are measured. The crack formation and propagation, as well as the AE events, increase gradually as the stress increases. Before the peak stress is reached, the acoustic emission count of each defect and filling model is basically positively correlated with the stress value.

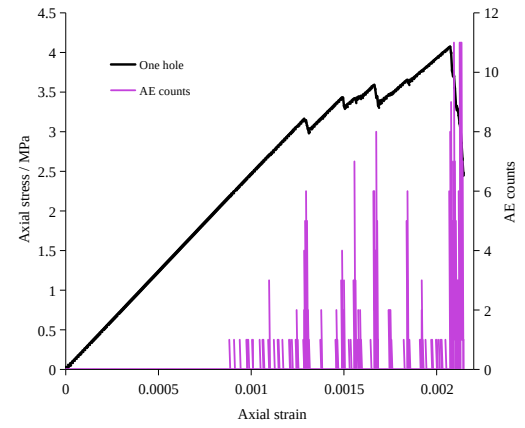

(a) Model B-1

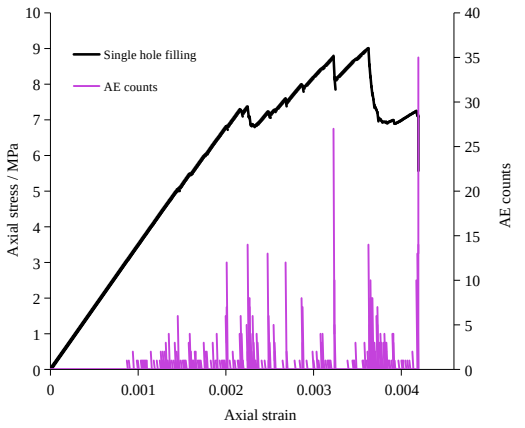

(b) Model B-2

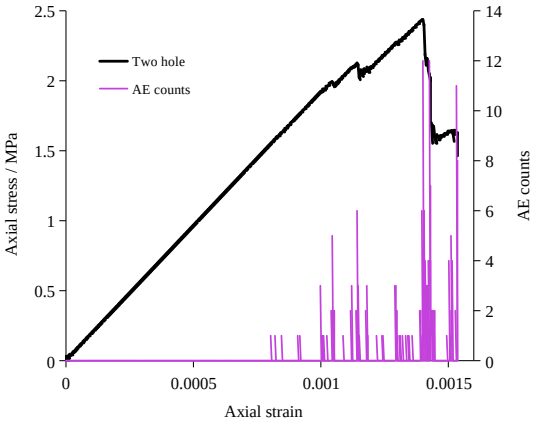

(c) Model C-1

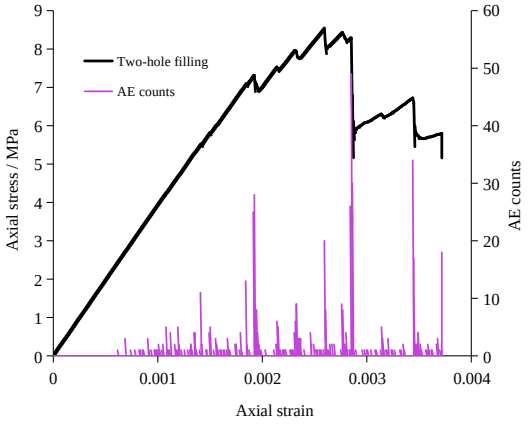

(d)Model C-2

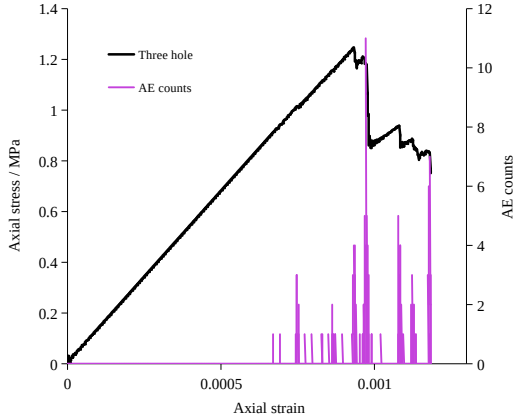

(e) Model D-1

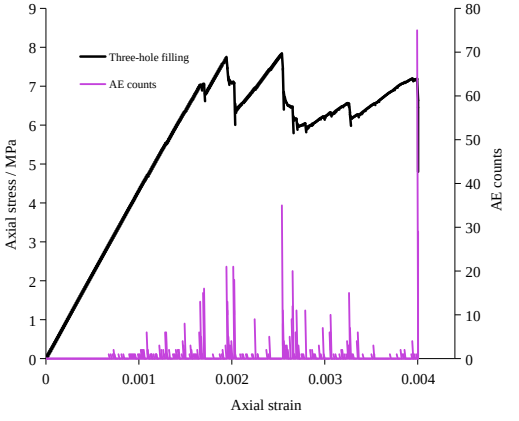

(f) Model D-2

Fig. 11 Distribution of stress-strain along with AE counts of models

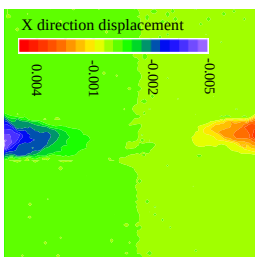

X direction displacement

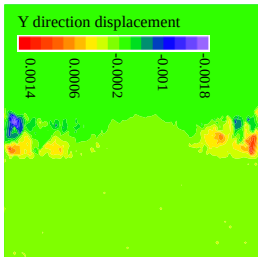

Y direction displacement

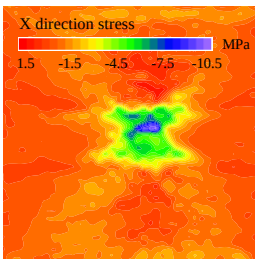

X direction stress

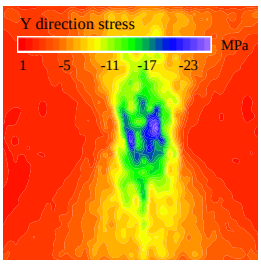

Y direction stress

Fig. 12 Displacement and stress field of model A after failure

The maximum number of AE events is noted near the peak value of the stress-strain curve. The peak values of stress and strain, as well as the range of AE counts, decrease as the number of holes increases, but the number of holes does not directly affect the initiation and size of AE signals. The strain value of the filled models does not change significantly when the first AE events occur. The peak stress of the filled models are much higher than that of the defect models, including the post peak stress stage, and the number of acoustic emission hits are also increased. The total number of AE shots for the filled model is larger than the one of the defective models.

Moreover, the maximum counts of AE increase as the number of the filling holes increases. The results show that after filling, the cracks of each model first occur in the coal sample with low strength and that the fillings have small effect on the generation of AE signals. However, they have a significant impact on AE counts. The distribution of AE counts of the filled models are complex especially in the post-peak phase, the internal crack of the samples expand rapidly before the failure of the models and the AE counts increase rapidly. The damage evolution of the models is gradually diffused into the rock sample with the increase of filling volume.

3.5 Distribution of displacement and stress fields after model failure for complete model

Fig. 12 shows the displacement and stress fields for model A after failure, where X and Y directions express the horizontal and vertical directions of the model, respectively. In the displacement field, the change of displacement to the left is represented by negative value, and the change to the right is represented by positive value; In the stress field, the positive value represents tensile stress and the negative value represents compressive stress (the same below). The displacement changes are mainly concentrated in the range of coal layer, while small displacement changes occur inside the upper and lower rock samples. In this model, the coal layer is subjected to vertical compression stress, resulting in a maximum vertical displacement of 1.8 mm and the horizontal displacement mainly develops in both ends of the coal body. When model A fails, the stress in horizontal direction is mainly accumulated in the coal layer at the center of the whole model, with a value of the maximum stress that reaches approximately 10.5 MPa. Small tensile stresses are mainly generated on the left and right sides of the model. Similarly, the stress accumulation in vertical direction is noted at the center of the model and it is in the form of a vertical bundle with two divergent ends. The maximum compressive stress at the center of the model is about 23 MPa.

3.6 Distribution of displacement and stress fields after model failure for defective and filled models

Fig. 13 shows the displacement field after failure of the models with defects and filling material. The displacement in both directions is noted around each hole. As the number of holes increases, both horizontal and vertical displacements decrease. When the displacement of the defective model D is very small, the model fails, showing that the quantity and area of defects controls the damage development. After the hole is completely filled, the displacement field becomes similar to the one of model A. Both ends of coal layer are extruded and stretched in the horizontal direction. In the vertical direction, the coal body and part of filling material are compressed. The displacement caused by compression is concentrated in both ends of the middle coal layer. Especially in the filled model D, the horizontal and vertical displacements of the model changes significantly when the model fails.

Fig.14 shows the distribution of stress field of the defective and filled models after failure. The stress concentration area is symmetrically accumulated on both sides of the square holes in both horizontal and vertical directions, but the values are larger in the vertical direction. Compared with model A, the stress concentration area of the defective models is distributed to the left and right sides of the outer holes, while the stress is small between the holes. Due to the large quantity and area of defects, the distribution of stress field for the defective model D changes greatly and the stress concentration area is mainly accumulated in the coal body among the three holes. The number and permutation of square holes change the distribution of stress field of the RCR combination, while the stress concentration range gradually moves outward and disperses. The maximum horizontal and vertical stress values decrease as the number of holes increases.

The stress distribution of the filled models at failure, shown in Fig.12(b), is similar to the one of model A, but the stress concentration area is slightly larger and the stress values are smaller in both directions. Compared with the defective models, the maximum stress values of the filled models in horizontal direction increase from 1.65 to 5.38 times, while in vertical direction they increase from 3.17 to 4.18 times. Hence, after filling the holes of the defective model, the stress value of the model is significantly improved and the strength of the RCR combination is enhanced.

4. Discussion

In this paper, the PFC2D particle flow program is used to systematically discuss six working conditions of the RCR models from the aspects of crack development, acoustic emission characteristics, contact force chain, stress field and displacement field distribution. However, in order to facilitate the research, this article assumes the shape of the hole defect as a common square. Other shapes and sizes are not studied.

Based on previous studies on the crack development and force chain distribution of square holes, it is concluded that the shape, size and location of the defect have a certain impact on the mechanical properties of the rock mass (Gui *et al.* 2017, Zhou *et al.* 2017, Huang *et al.* 2017, Xia *et al.* 2020). More specifically, Xia *et al*., 2020, proved that, when the uniform square defect was filled to improve the bearing capacity of the rock, the maximum compressive stresses were distributed on the left and right sides of the hole; Zhou *et al*., 2017, concluded that two rectangular

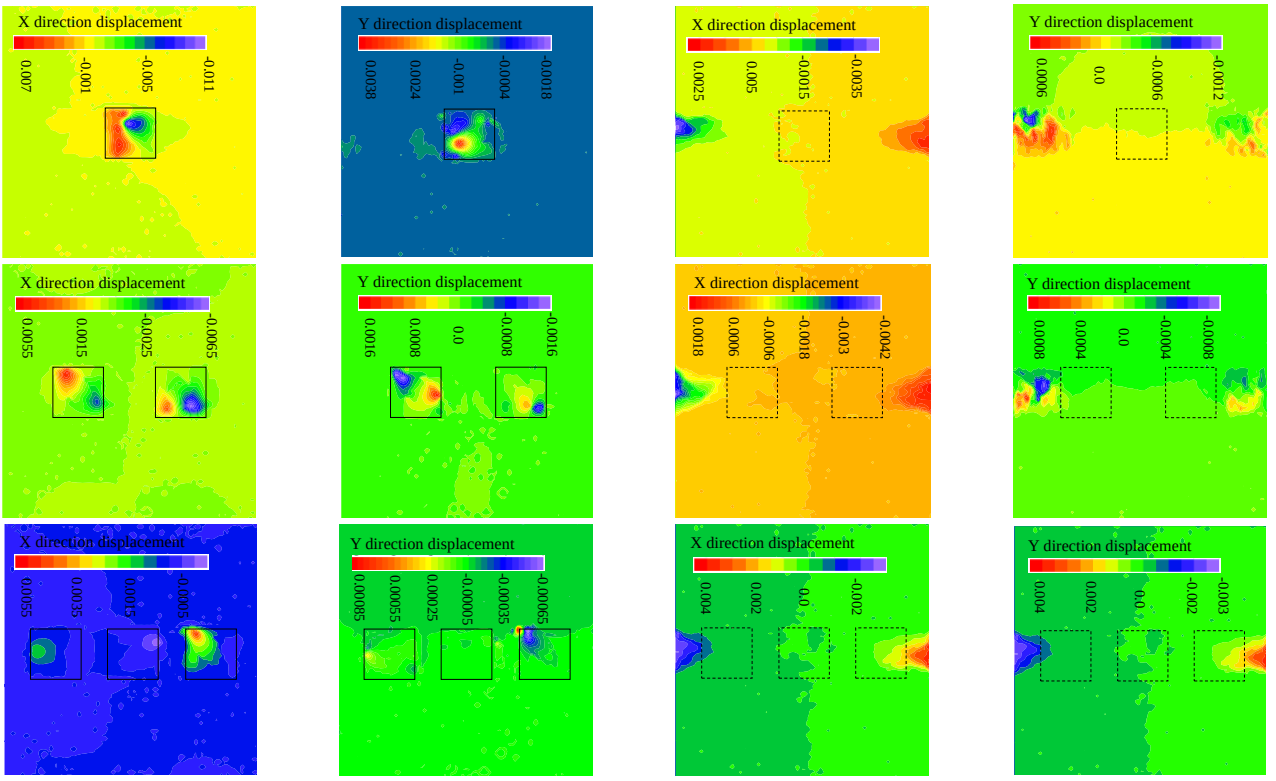

(a) Displacement field of model with defects (b) Displacement field of model after fillings

Fig. 13 Displacement field after models failure

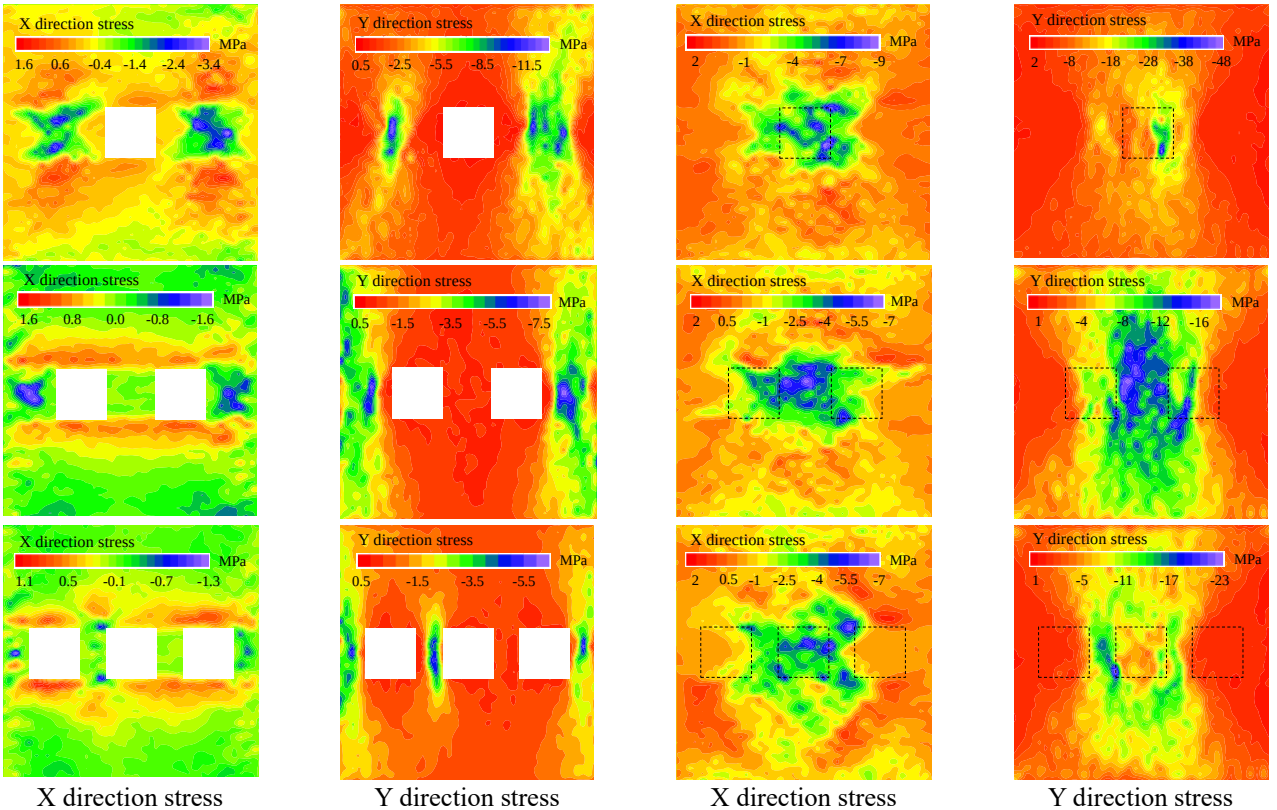

(a) Stress field of model with defects (b) Stress field of model after fillings

Fig. 14 Stress field after model failure

cavities degraded the mechanical properties of the rock more severely than a single cavity. However, the model setup of the present paper is different from the ones adopted in the aforementioned publications, as the fine-scale damage characteristics of square hole defects in weak layers are consistent with the damage laws. The main research purpose of this paper is to analyze the influence of the defects in the weak layer on the mechanical properties of the combination, and identify the most important factors in order to extend the research in the future with other shapes and sizes of defects.

Moreover, in order to consider the maximum size of the weak interlayer defects and distinguish better the upper and lower hard rock layers, the height of the defects in this article is assumed to coincide with the thickness of the weak layer. In the actual stratum, the defects can also be smaller, surrounded by the weak interlayer without being in contact with the hard rock. This also provides a reference for studying the effect of weak interlayer on stress deformation during underground tunnel excavation on a large scale (Huang *et al.* 2013, Aksoy *et al.* 2012).

5. Conclusions

- The defects in a weak interlayer have a great impact on the mechanical properties of RCR combination samples, reducing the values of the peak stress and strain, as well as the elastic modulus. After the holes are filled, the mechanical properties of the RCR combination samples are improved significantly.
- The strain developed in the defective models, when the initial crack appears and when the models fail, are both smaller than the ones of the complete model without defects. The more defects exist, the earlier the cracks occur. The final strain of the filled models, the total number of cracks after failure and the crack initiation stress are larger than those of the defective models, indicating that the filled models can sustain larger loads. After filling, the appearance and development of new cracks in the model are restrained and the damage evolution of the model is mainly generated in the coal layers and gradually spread into the rock samples.
- When the complete RCR combination fails, the compression deformation occurs at both ends of the coal layer, while the internal displacement of the rock sample hardly changes. The displacement of the coal layer expands to the material around the hole. The quantity and area of the holes controls the development of failure. The more defects, the easier the RCR combination models fail.
- The presence of holes changes the distribution of contact force and the stress concentration range and size. The stress of the defective models is mainly concentrated in the coal body on both sides of the holes in contrast to the complete combination model, which presents a smaller range and lower stress value. The stress concentration range of the filled models expands and the stress value increases. After filling the defective models, the bearing capacity of the RCR combination is improved significantly.

Acknowledgments

The research described in this paper was financially supported by the National Natural Science Foundation of China (NO. U1704243), Key Scientific Research Project Plan of Henan Higher Education Institutions (NO.17A410002), The Doctoral Innovation Fund of North China University of Water Resource and Electric Power, and The Project of High Level Talents in North China University of Water Resource and Electric Power (NO.201518).

References

Aksoy, C.O., Ogul, K., Topal, I., Ozer, S.C., Ozacar, V. and Posluk, E. (2012), "Numerical modeling of non-deformable support in swelling and squeezing rock", *Int. J. Rock Mech. Min. Sci.*, **52**, 61-70. https://doi.org/10.1016/j.ijrmms.2012.02.008.

Ayatollahi, M.R. and Akbardoost J. (2014), "Size and Geometry Effects on Rock Fracture Toughness: Mode I Fracture", *Rock Mech. Rock Eng.*, **47**, 677-687. https://doi.org/10.1007/s00603-013-0430-7.

Bahaaddini, M., Sharrock, G. and Hebblewhite, B.K. (2013), "Numerical investigation of the effect of joint geometrical parameters on the mechanical properties of a non-persistent jointed rock mass under uniaxial compression", *Comput. Geotech.*, **49**, 206-225. https://doi.org/10.1016/j.compgeo.2012.10.012.

Bahrani, N. and Kaiser, P.K. (2016), "Numerical investigation of the influence of specimen size on the unconfined strength of defected rocks", *Comput. Geotech.*, **77**, 56-67. https://doi.org/10.1016/j.compgeo.2016.04.004.

Brandtner-Hafner, M. (2021), "Structural Safety Evaluation of Adhesive Bonds: A Fracture Analytical Approach", *Eng. Fail. Anal.*, **123**, 105289. https://doi.org/10.1016/j.engfailanal.2021.105289.

Castro-Filgueira, U., Alejano, L.R., Arzúa, J. and Ivars, D.M. (2017), "Sensitivity analysis of the micro-parameters used in a PFC analysis towards the mechanical properties of rocks", *Proc. Eng.*, **191**, 488-495. https://doi.org/10.1016/j.proeng.2017.05.208.

Cauvin, A. and Testa, R.B. (1999), "Damage mechanics: Basic variables in continuum theories", *Int. J. Solids Struct.*, **36**, 747-761. https://doi.org/ 10.1016/S0020-7683(98)00044-4.

Chen, S.J., Xia, Z.G. and Feng, F. (2020), "Numerical simulation of strength, deformation, and failure characteristics of rock with fissure hole defect", *Adv. Mater. Sci. Eng.*, **2020**, 7048645. https://doi.org/10.1155/2020/7048645.

Cundall, P.A. and Strack, O.D. (1979), "A discrete numerical model for granular assemblies", *Geotechnique*, **29**(1), 47-65. https://doi.org/10.1680/geot.1979.29.1.47.

Eberhardt, E., Stead, D.,Stimpson, B. (1998), "Identifying crack initiation and propagation thresholds in brittle rock", *Can. Geotech. J.*, **35**(2), 222-233. https://doi.org/10.1139/cgj-35-2-222.

Esterhuizen, G.S., Dolinar, D.R.and Ellenberger, J.L. (2011), "Pillar strength in underground stone mines in the United States", *Int. J. Rock Mech. Min. Sci.*, **48**, 42-50. https://doi.org/10.1016/j.ijrmms.2010.06.003.

Fairhurst, C.E. and Hudson, J.A. (1999), "Draft ISRM suggested method for the complete stressstrain curve for the intact rock in uniaxial compression", *Int. J. Rock Mech. Min. Sci. Geomech. Abstr.*, **36**(3), 281-289. https://doi.org/10.1016/S0148-9062(99)00006-6.

Fakhimi, A., Carvalho, F., Ishida, T. and Labuz, J.F. (2002), "Simulation of failure around a circular opening in rock", *Int. J. Rock Mech. Min. Sci.*, **39**(2), 507-515. https://doi.org/10.1016/S1365-1609(02)00041-2.

Gui, Y.L., Zhao, Z.Y., Zhang, C. and Ma, S.Q. (2017), "Numerical investigation of the opening effect on the mechanical behaviours in rocks under uniaxial loading using hybrid

continuum discrete element method", *Comput. Geotech.*, **90**, 55-72. https://doi.org/10.1016/j.compgeo.2017.05.021.

Guo, W.Y., Tan, Y.L., Yu, F.H., Zhao, T.B., Hu, S.C., Huang, D.M. and Qin, Z. (2018), "Mechanical behavior of rock-coal-rock specimens with different coal thicknesses", *Geomech. Eng.*, **15**(4), 1017-1027. https://doi.org/10.12989/gae.2018.15.4.1017.

Hadjigeorgiou, J., Esmaieli, K. and Grenon, M. (2009), "Stability analysis of vertical excavations in hard rock by integrating a fracture system into a PFC model", *Tunn. Undergr. Space Technol.*, **24**, 296-308. https://doi.org/10.1016/j.tust.2008.10.002.

Haimson, B. and Kovacich, J. (2003), "Borehole instability in high-porosity Berea sandstone and factors affecting dimensions and shape of fracture-like breakouts", *J. Eng. Geol.,* **69**, 219-231. https://doi.org/10.1016/S0013-7952(02)00283-1.

Hawkes, I. and Mellor, M. (1970), "Uniaxial testing in rock mechanics laboratories", *Eng. Geol.*, **4**, 177-285. https://doi.org/10.1016/0013-7952(70)90034-7.

Hazzard, J.F. and Young, R.P. (2000), "Simulating acoustic emissions in bonded-particle models of rock", *Int. J. Rock Mech. Min. Sci.*, **37**(5), 867-872. https://doi.org/10.1016/S1365-1609(00)00017-4.

Helgeson, D.E. and Aydin, A. (1991), "Characteristics of joint propagation across layer interfaces in sedimentary rocks", *J. Struct. Geol.*, **13**(8), 897-911. https://doi.org/10.1016/0191-8141(91)90085-W.

Hillerborg, A., Modéer, M. and Petersson, P.E. (1976), "Analysis of crack formation and crack growth in concrete by means of fracture mechanics and finite elements", *Cement Concrete Res.*, **6**, 773-782. https://doi.org/10.1016/0008-8846(76)90007-7.

Hillerborg, A. (1985), "The theoretical basis of a method to determine the fracture energy GF of concrete", *Mater. Struct.*, **18**, 291-296. https://doi.org/10.1007/BF02472919.

Holt, R.M., Kjolaas J., Larsen, I., Li, L., Pillitteri, A.G. and Sonstebo, E.F. (2005), "Comparison between controlled laboratory experiments and discrete particle simulations of the mechanical behaviour of rock", *Int. J. Rock Mech. Min. Sci.*, **42**, 985-995. https://doi.org/10.1016/j.ijrmms.2005.05.006.

Huang, F., Zhu, H.H., Xu, Q.W., Cai, Y.C. and Zhuang, X.Y. (2013), "The effect of weak interlayer on the failure pattern of rock mass around tunnel-scaled model tests and numerical analysis", *Tun. Under. Sp. Tech.*, **35**, 207-218. http://dx.doi.org/10.1016/j.tust.2012.06.014.

Huang, Y.H., Yang, S.Q., Ranjith P.G. and Zhao, J. (2017), "Strength failure behavior and crack evolution mechanism of granite containing pre-existing non-coplanar holes: Experimental study and particle flow modeling", *Comput. Geotech.*, **88**, 182-198. http://dx.doi.org/10.1016/j.compgeo.2017.03.015.

International Society for Rock Mechanics (ISRM) (1981), "Suggested methods for the quantitative description of discontinuities in rock masses", *Rock Characterization, Testing and Monitoring-ISRM Suggested Methods*, Pergamon Press, Oxford, 3-52.

Janeiro, R.P. and Einstein, H.H. (2010), "Experimental study of the cracking behavior of specimens containing inclusions (under uniaxial compression)", *Int. J. Fract. Eng.*, **164**(1), 83-102. https://doi.org/10.1007/s10704-010-9457-x.

Jespersen, C., MacLaughlin, M., and Hudyma, N. (2010), "Strength, deformation modulus and failure modes of cubic analog specimens representing macroporous rock", *Int. J. Rock Mech. Min. Sci.*, **47**, 1349-1356. https://doi.org/10.1016/j.ijrmms.2010.08.015.

Kim, J.S., Lee, K.S., Cho, W.J., Choi, H.J. and Cho, G.C. (2015), "A comparative evaluation of stress-strain and acoustic emission methods for quantitative damage assessments of brittle rock", *Rock Mech. Rock Eng.*, **48**, 495-508. https://doi.org/10.1007/s00603-014-0590-0.

Klein, E. and Reuschle, T. (2004), "A pore crack model for the mechanical behaviour of porous granular rocks in the brittle deformation regime", *Int. J. Rock Mech. Min. Sci.*, **41**, 975-986. https://doi.org/10.1016/j.ijrmms.2004.03.003.

Komijani, M., Gracie, R. and Yuan, Y. (2020), "Simulation of fracture propagation induced acoustic emission in porous media", *Eng. Fract. Mech.*, **229**, 106950. https://doi.org/10.1016/j.engfracmech.2020.106950.

Komijani, M. and Gracie, R. (2019), "Enriched mixed finite element models for dynamic analysis of continuous and fractured porous media", *Comput. Methods Appl. Mech. Eng.*, **343**, 74-99. https://doi.org/10.1016/j.cma.2018.08.011.

Komurlu, E., Kesimal, A. and Demir, S. (2016), "Experimental and numerical analyses on determination of indirect (splitting) tensile strength of cemented paste backfill materials under different loading apparatus", *Geomech. Eng.*, **10**(6), 775-791. https://doi.org/10.12989/gae.2016.10.6.775.

Kranz, R. L. (1979), "Crack-crack and crack-hole interactions in stressed granite", *Int. J. Rock Mech. Min. Sci.*, **16**, 37-47. https://doi.org/10.1016/0148-9062(79)90773-3.

Lajtai, E.Z. (1974), "Brittle fracture in compression", *Int. J. Fract.*, **10**(4), 525-536. https://doi.org/10.1007/BF00155255.

Liu, H.D., Li, L.D., Zhao, S.L. and Hu, S.H. (2019a), "Complete stress-strain constitutive model considering crack model of brittle rock", *Environ. Earth Sci.*, **78**, 629. https://doi.org/10.1007/s12665-019-8643-z.

Liu, W.R., Yuan, W., Yan, Y.T. and Wang, X. (2019b), "Analysis of acoustic emission characteristics and damage constitutive model of coal-rock combined body based on particle flow code", *Symmetry*, **11**(8), 1040. https://doi.org/10.3390/sym11081040.

Liu, X.S., Tan, Y.L., Ning, J.G., Lu, Y.W. and Gu, Q.H. (2018), "Mechanical properties and damage constitutive model of coal in coal-rock combined body", *Int. J. Rock Mech. Min. Sci.*, **110**, 140-150. https://doi.org/10.1016/j.ijrmms.2018.07.020.

Lisjak, A. and Grasselli, G. (2014), "A review of discrete modeling techniques for fracturing processes in discontinuous rock mass", *J. Rock Mech. Geotech. Eng.*, **6**(4), 301-314. https://doi.org/10.1016/j.jrmge.2013.12.007.

Lollino, G., Giordan, D., Thuro, K., Carranza-Torres, C., Wu, F., Marinos, P. and Delgado, C. (2015), *Engineering Geology for Society and Territory Volume 6: Applied Geology for Major Engineering Projects*, Springer International Publishing, Cham, Canton of Zug, Switzerland.

Marinelli, F. and Buscarnera, G. (2019), "Anisotropic breakage mechanics: From stored energy to yielding in transversely isotropic granular rocks", *J. Mech. Phys. Solids*, **129**, 1-18. https://doi.org/10.1016/j.jmps.2019.04.013.

Martin, C.D., Kaiser, P.K. and Christiansson, R. (2003), "Stress, instability and design of underground excavations", *Int. J. Rock Mech. Min. Sci.*, **40**, 1027-1047. https://doi.org/10.1016/S1365-1609(03)00110-2.

Mikl-Resch, M. J., Antretter, T., Gimpel, M., Kargl, H., Pittino, G., Tichy, R., Ecker, W. and Galler,R. (2015), "Numerical calibration of a yield limit function for rock materials by means of the Brazilian test and the uniaxial compression test", *Int. J. Rock Mech. Min.*, **74**, 24-29. http://dx.doi.org/10.1016/j.ijrmms.2014.12.001.

Molladavoodi, H. and Mortazavi, A. (2011), "A damage-based numerical analysis of brittle rocks failure mechanism", *Finite Elem. Anal. Des.*, **47**, 991-1003. https://doi.org/10.1016/j.finel.2011.03.015.

Mondal, S., Olsen-Kettle, L.and Gross, L. (2019), "Simulating damage evolution and fracture propagation in sandstone containing a preexisting 3-D surface flaw under uniaxial compression", *Int. J. Numer Anal. Met.*, **43**(7), 1448-1466. https://doi.org/10.1002/nag.2908.

Moradi, P., Asadi, M.J., Ebrahimzadeh, N. and Yarahmadi, B. (2021), "Ilam tunnels inspection, maintenance, and

rehabilitation: A case study", *Tunn. Under. Sp. Tech.*, **110**, 103814. https://doi.org/10.1016/j.tust.2021.103814.
Nick, H.M., Paluszny, A., Blunt, M.J. and Matthai, S.K. (2011), "Role of geomechanically grown fractures on dispersive transport in heterogeneous geological formations", *Phys. Rev. E*, **84**(5), 056301. https://doi.org/10.1103/PhysRevE.84.056301.
Park, C.H. and Bobet, A. (2009), "Crack coalescence in specimens with open and closed flaws: a comparison", I*nt. J. Rock Mech. Min. Sci.*, **46**(5), 819-829. https://doi.org/10.1016/j.ijrmms.2009.02.006.
Pelli, F., Kaiser, P.K. and Morgenstern, N.R. (1991), "An interpretation of ground movements recorded during construction of ground movements recorded during construction of the Donkin-Morien tunnel", *Can. Geotech. J.*, **28**(28), 239-254. https://doi.org/10.1016/0148-9062(92)91539-h.
Pepe, G., Mineo, S., Pappalardo, G. and Cevasco, A. (2017), "Relation between crack initiation-damage stress thresholds and failure strength of intact rock", *Bull. Eng. Geol. Environ.*, **77**(2), 709-724. https://doi.org/10.1007/s10064-017-1172-7.
Potyondy D.O. (2015), "The bonded-particle model as a tool for rock mechanics research and application: current trends and future directions", *Geosyst. Eng.*, **18**(1), 1-28. https://doi.org/10.1080/12269328.2014.998346.
Potyondy, D.O. and Cundall, P.A. (2004), "A bonded-particle model for rock", *Int. J. Rock Mech. Min. Sci.*, **41**(8), 1329-1364. https://doi.org/10.1016/j.ijrmms.2004.09.011.
Sharafisafa, M., Aliabadian, Z., Tahmasebinia, F. and Shen, L.M. (2020), "A comparative study on the crack development in rock-like specimens containing unfilled and filled flaws", *Eng. Fract. Mech.*, **241**, 107405. https://doi.org/10.1016/j.engfracmech.2020.107405.
Strmsvik, H. and Gammelster, B. (2020), "Investigation and assessment of pre-grouted rock mass", *B. Eng. Geol. Environ.*, **79**, 2543-2560. https://doi.org/10.1007/s10064-019-01722-9.
Tian, W.L. and Yang, S.Q. (2017), "Experimental and numerical study on the fracture coalescence behavior of rock-like materials containing two non-coplanar filled fissures under uniaxial compression", *Geomech. Eng.*, **12**(3), 541-560. https://doi.org/10.12989/gae.2017.12.3.541.
Tropeano, M., Sabato, L. and Pieri, P. (2002), "Filling and cannibalization of a foredeep: The Bradanic Trough, Southern Italy", *Geol. Soc. of London, Spec. Publ.*, **191**(1), 55-79. https://doi.org/10.1144/GSL.SP.2002.191.01.05.
Vasarhelyi, B. and Bobet, A. (2000), "Modeling of crack initiation, propagation and coalescence in uniaxial compression", *Rock Mech. Rock Eng.*, **33**(2), 119-139. https://doi.org/10.1007/s006030050038.
Wang, D.B., Bian, X.B., Qin, H., Sun, D.L. and Yu, B. (2021), "Experimental investigation of mechanical properties and failure behavior of fluid-saturated hot dry rocks", *Nat. Resour. Res.*, **30**(1), 289-304. https://doi.org/10.1007/s11053-020-09760-x.
Wang, X., Wen, Z.J. and Jiang, Y.J. (2016), "Time-space effect of stress field and damage evolution law of compressed coal-rock", *Geotech. Geol. Eng.*, **34**(6), 1933-1940. https://doi.org/10.12989/gae.2020.21.3.259.
Wong, R.H.C., Lin, P. and Tang, C.A. (2006), "Experimental and numerical study on splitting failure of brittle solids containing single pore under uniaxial compression", *Mech. Mater.*, **38**(1-2), 142-159. https://doi.org/10.1016/j.mechmat.2005.05.017.
Wu, M., Wang, J., Russell, A. and Cheng, Z. (2020), "DEM modelling of mini-triaxial test based on one-to-one mapping of sand particles", *Géotechnique*, **71**(8), 1-14. https://doi.org/10.1680/jgeot.19.P.212.
Wu, M., Huang, R., and Wang, J. (2021), "DEM simulations of cemented sands with a statistical representation of micro-bond parameters", *Powder Technol.*, **379**, 96-107. https://doi.org/10.1016/j.powtec.2020.10.047.
Xia, Z.G., Chen, S.J., Liu, X. Z. and Sun, R. (2020), "Strength characteristics and fracture evolution of rock with different shapes inclusions based on particle flow code", *Geomech. Eng.*, **22**(5), 461-473. https://doi.org/10.12989/gae.2020.22.5.461.
Yang, B., Jiao, Y. and Lei, S. (2006), "A study on the effects of microparameters on macroproperties for specimens created by bonded particles", *Eng. Computation.*, **23**(6), 607-631. https://doi.org/10.1108/02644400610680333.
Yang, S.Q., Huang, Y.H., Tian, W.L. and Zhu, J.B. (2017), "An experimental investigation on strength, deformation and crack evolution behavior of sandstone containing two oval flaws under uniaxial compression", *Eng. Geol.*, **217**, 35-48. http://dx.doi.org/10.1016/j.enggeo.2016.12.004.
Yin, D.W., Chen, S.J., Chen, B., Liu, X.Q. and Ma, H.F. (2018), "Strength and failure characteristics of the rock coal combined body with single joint in coal", *Geomech. Eng.*, **15**(5), 1113-1124. https://doi.org/10.12989/gae.2018.15.5.1113.
Zhou, Z.L., Tan, L.H., Cao, W.Z., Zhou, Z.Y. and Cai, X. (2017), "Fracture evolution and failure behaviour of marble specimens containing rectangular cavities under uniaxial loading", *Eng. Fract. Mech.*, **184**, 183-201. https://doi.org/10.1016/j.engfracmech.2017.08.029.
Zuo, J.P., Xie, H.P., Wu, A.M. and Liu, J.F. (2011), "Investigation on failure mechanisms and mechanical behaviors of deep coal-rock single body and combined body", *Chin. J. Rock Mech. Eng.*, **30**(1), 84-92. https://doi.org/10.3724/SP.J.1077.2011.00271.

CC